

Quantum effects on the multiphoton dissociation of a diatomic molecule

Robert Graham and Michael Höhnerbach

Fachbereich Physik, Universität Gesamthochschule Essen, D-4300 Essen 1, Germany

(Received 2 August 1990)

The chaotic vibrations of a diatomic molecule in an intense monochromatic electromagnetic field are classically and quantum mechanically analyzed. It is shown that the driven motion in a Morse potential is accurately described by a return map—the Morse map, whose derivation in various degrees of approximation is presented in detail. The quantization of the map is also considered. The quantized map, though acting on states in the energy range of bound states only, is shown to be influenced by intermediate states above the dissociation threshold, i.e., effects of the continuum are incorporated. Detailed numerical results are presented and various localization mechanisms are discussed and compared.

I. INTRODUCTION

After the development of efficient lasers in the infrared and the discovery of highly specific laser-induced chemical reactions, the experimental and theoretical study of multiphoton excitation and dissociation of molecules has grown into a vast field of research. For a review see, e.g., Ref. 1. Recently, new impetus was given to the theoretical side of this field by an increased understanding of the crucial features of the underlying dynamics at least in a classical description: it was recognized that classically the dynamics (vibrations and rotations) are chaotic, and that the basic mechanism leading to multiple-photon excitation and dissociation is the chaotic but deterministic diffusion of the molecular energy.² Therefore the methods and concepts used in the study of chaotic systems have increasingly been applied.

Here we wish to report our work on periodically driven molecular vibrations in the Morse potential, in a classical description *and* its quantum counterpart. As a new basic tool we introduce in our study a Poincaré map, which is unusual in that it is *not* based on the stroboscopic map over one oscillation period of the external driving infrared field, but instead is based on the molecular oscillation itself. A similar map was recently used in studies of the microwave excitation of Rydberg atoms.³ The method is designed to combine advantages of the two main theoretical methods which have been applied to this problem in earlier work. These methods are (i) the stroboscopic classical map in periods of the external field or the corresponding quantum map over one external period, which is based on the Floquet theorem; (ii) the quasis resonant or rotating frame approximation which treats the multiple-photon excitation as a stepwise process in which only those vibrational levels participate appreciably which are approximately spaced a photon energy apart.

The main advantage of method (i) consists in the use of a map instead of the underlying continuous-time dynamics. In fact, it was this simple but ingenious idea due to Poincaré and its easy implementation on modern computers that was the main driving force behind the break-

through in our present understanding of chaotic dynamical systems. A disadvantage of this method is the fact that neither classically nor quantum mechanically is the stroboscopic map known explicitly and has to be constructed numerically.

The method we shall develop below leads to an explicit map, both classically and quantum mechanically, and therefore avoids this disadvantage.

Method (ii)—the quasis resonant approximation mentioned above—is designed for the quantum problem only. It also avoids the disadvantage of the first method by simplifying the Schrödinger equation, keeping only near-resonant molecular states, and, in addition, neglecting “counterrotating terms” such that the effective Hamiltonian is no longer time dependent. The Schrödinger equation is then solved by diagonalizing the effective Hamiltonian. The advantage of this well-known method (Ref. 1) is the reduction of the number of relevant states by keeping only those of highest physical relevance, thereby decreasing the duration of numerical computations. The method we shall present here exploits the restriction to near-resonant states achieved by the quasis resonant approximation already in the classical domain and shares the simplifications of that approximation in the quantum domain, however, at the same time maintaining the description of the dynamics in terms of a map.

Recently, a number of studies have been devoted to the quantum-mechanical problem of molecular vibrations in a Morse potential driven by a monochromatic external field. These studies are based on direct numerical solutions of the Schrödinger equations. Walker and Preston⁴ compared the classical and quantum dynamics for moderate excitation far below the dissociation threshold. Goggin and Milonni⁵ extended this work to higher excitation and longer time, including effects of the continuum. Leforestier and Wyatt⁶ used the Floquet theory and an optical potential approach to describe the decay into the continuum, while Tanner and Maricq⁷ used Floquet theory and neglected the continuum comparing their results with a direct simulation via a fast-Fourier-transform grid method. Flosnik and Wyatt⁸ eliminated the continu-

um and derived an integro-differential equation for the wave function in the bound subspace of the unperturbed Hamiltonian, which is solved after approximations on the integral kernel assuming short memory times.

The approach described here differs from these works mainly by the fact that an important part of the problem is solved already in the classical domain, before the quantization is performed. This procedure is justified in the quasiclassical WKB limit. Indeed quasiclassical Bohr-Sommerfeld quantization in classically integrable Hamiltonian systems is based on and requires the solution of the classical dynamics for one round-trip of the system. Similarly, the map on which the quantization is based here describes one molecular vibration period. A short presentation of our map and some results obtained from it are given in Ref. 9.

The manuscript is organized as follows. In Sec. II we specify the classical model and introduce the action and angle variables of the free oscillations and of the unbound motion above the dissociation threshold. In Sec. III we derive the dynamical map over one vibration period (Morse map) and compare it with the more conventional stroboscopic map over a period of the external field. Conclusions which can be drawn either directly from this map or by comparing it with the standard map are also given there. Section IV considers the quantization of the map, and summarizes the new effects it describes. In Sec. V we present and discuss our numerical results for time-dependent expectation values, Floquet states, and the dissociation probability. Section VI summarizes our conclusions.

II. CLASSICAL MODEL

A. Hamiltonian

We wish to consider the pure vibrational motion of a diatomic molecule for a fixed electronic configuration and under the assumption that rotational motion is not excited. Under these assumptions the molecular potential may be described by a Morse potential¹⁰

$$V(r) = D(1 - e^{-\alpha(r-r_0)})^2, \quad (2.1)$$

where D is the dissociation energy, r_0 is the nuclear distance at equilibrium, and α^{-1} is the range of the molecular potential. Hydrogenhalogenides HF and HCl are examples where our assumptions are well satisfied. Their parameters D , α , and r_0 can be found in Ref. 11. The Hamiltonian of the molecule in an external homogeneous monochromatic electromagnetic field of frequency ω_0 can be taken in the form

$$H = \frac{[P - eA(\tau)]^2}{2M} + V(r). \quad (2.2)$$

Here we neglected the possibility of an r -dependent screening of the effective charge e interacting with the external field. In Eq. (2.2) M is the reduced mass and

$$A(t) = \frac{1}{\omega_0} F \sin \omega_0 t \quad (2.3)$$

is the vector potential, where F is the amplitude of the externally applied electric field at frequency ω_0 . After scaling all variables according to

$$\begin{aligned} x &= r - r_0, \\ p &= P / \sqrt{2DM}, \\ t &= \Omega_0 \tau, \end{aligned} \quad (2.4)$$

where $\Omega_0 = \alpha \sqrt{2D/M}$ is the frequency of small oscillations, the Hamiltonian takes the form

$$H = \frac{[P - (g/\omega) \sin \omega t]^2}{2} + \frac{1}{2}(1 - e^{-x})^2 \quad (2.5)$$

and contains the two dimensionless parameters

$$g = \frac{eF}{2D\alpha}, \quad \omega = \frac{\omega_0}{\Omega_0}, \quad (2.6)$$

which are the external field amplitude and its frequency in molecular units. The oscillations of the unperturbed molecule ($g=0$) are described by (2.5) in a parameter-free fashion. In this case ($g=0$) the separatrix at $H = \frac{1}{2}$, $p = \pm [1 - (1 - e^{-x})^2]^{1/2}$, separates bound states ($0 \leq H < \frac{1}{2}$) from dissociated states ($H > \frac{1}{2}$).

B. Action-angle variables for bound motion

It is well known that motions in the unperturbed Morse potential ($g=0$) are regular and action-angle variables can be determined explicitly.¹² These variables define useful coordinates also for the description of the perturbed motion.^{13,5}

The action variable I is defined as usual by

$$I = \frac{1}{2\pi} \oint p dx, \quad (2.7)$$

which yields for the unperturbed bound motion

$$I = 1 - [1 - p^2 - (1 - e^{-x})^2]^{1/2} \quad (2.8)$$

for $0 \leq I \leq 1$. This equation may be solved for p and then compared with $p = \partial S(I, x) / \partial x$ in order to determine the generating function S of the canonical transformation $(x, p) \rightarrow (\theta, I)$. Then $\theta = \partial S(I, x) / \partial I$ may be used to obtain explicitly

$$\theta = \theta_0 + \arcsin \left[\frac{e^x(1-I)^2 - 1}{(2I - I^2)^{1/2}} \right]. \quad (2.9)$$

After solving for (x, p) we obtain, for $0 \leq I \leq 1$,

$$\begin{aligned} x &= \ln \left[\frac{1 - [2H_0^<(I)]^{1/2} \cos \theta}{1 - 2H_0^<(I)} \right] = x(I, \theta), \\ p &= [1 - 2H_0^<(I)]^{1/2} \frac{[2H_0^<(I)]^{1/2} \sin \theta}{1 - [2H_0^<(I)]^{1/2} \cos \theta} = p(I, \theta). \end{aligned} \quad (2.10)$$

Here we have chosen $\theta_0 = \pi/2$, which implies that $\theta=0$ in the turning point $p=0$ at the minimal nuclear distance. $H_0^<(I)$ is the unperturbed Hamiltonian for the bound motion expressed by the action variable I ,

$$H_0^<(I) = I - \frac{I^2}{2}. \quad (2.11)$$

The value of the action variable at the separatrix of the unperturbed motion is $I=1$. Now the full Hamiltonian, for $0 \leq I \leq 1$, can be expressed as

$$H(I, \theta, t) = H_0^<(I) - \frac{g}{\omega} p(I, \theta) \sin \omega t + \frac{g^2}{2\omega^2} \sin^2 \omega t. \quad (2.12)$$

We may note the invariance of this Hamiltonian under the symmetry transformation

$$I \rightarrow I, \quad \theta \rightarrow -\theta, \quad t \rightarrow t + \pi/\omega. \quad (2.13)$$

For future purposes it is also useful to present $p(I, \theta)$ as a Fourier series, for $0 \leq I \leq 1$,

$$p(I, \theta) = 2 \sum_{m=1}^{\infty} W_m(I) \sin m \theta \quad (2.14)$$

with

$$W_m(I) = [1 - 2H_0^<(I)]^{1/2} \left[\frac{1 - [1 - 2H_0^<(I)]^{1/2}}{1 + [1 - 2H_0^<(I)]^{1/2}} \right]^{m/2}. \quad (2.15)$$

C. Extension to unbound motion

In the domain of unbound motion $H > \frac{1}{2}$, $I > 1$ we define a new canonical transformation formally extending Eqs. (2.10), by

$$x = \ln \left[\frac{-1 + [2H_0^>(I)]^{1/2} \cosh \psi}{2H_0^>(I) - 1} \right], \quad (2.16)$$

$$p = [2H_0^>(I) - 1]^{1/2} \frac{[2H_0^>(I)]^{1/2} \sinh \psi}{[2H_0^>(I)]^{1/2} \cosh \psi - 1},$$

where $I > 1$ and $-\infty < \psi < +\infty$, and where $H_0^>(I)$ is the function defined for $I > 1$ by

$$H_0^>(I) = \frac{1}{2} + |H_0^<(I) - \frac{1}{2}| = 1 - I + \frac{1}{2}I^2. \quad (2.17)$$

In fact, inserting the transformation (2.16) in the unperturbed Hamiltonian, Eq. (2.5) for $g=0$, one finds that $H_0(I) = H_0^>(I)$ for $I > 1$. Therefore the transformations (2.10) and (2.16) together define action-angle variables for the bound *and* the unbound motion with the Hamiltonian

$$H_0(I) = \begin{cases} H_0^<(I) & \text{if } 0 \leq I \leq 1 \\ H_0^>(I) & \text{if } 1 \leq I \leq \infty \end{cases}. \quad (2.18)$$

This function is shown in Fig. 1.

The full Hamiltonian may then generally be written in the form (2.12) with $H_0^<(I)$ replaced by $H_0(I)$. The Fourier series (2.15) for $0 \leq I \leq 1$ is replaced by a Fourier integral, for $1 \leq I < \infty$,

$$p(I, \psi) = 2 \int_0^{\infty} d\mu W_\mu(I) \sin \mu \psi + \sqrt{2H_0(I) - 1} \operatorname{sgn}(\psi), \quad (2.19)$$

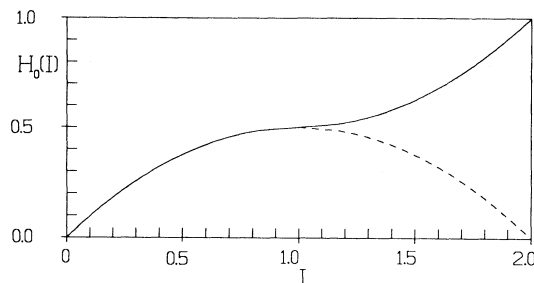


FIG. 1. The Hamiltonian $H_0(I)$ (2.18) for the bound and unbound motion. The dashed line is $H_0^<(I)$ formally extended for $I > 1$.

where $\operatorname{sgn}(\psi) = \psi/|\psi|$. The Fourier transform $W_\mu(I)$ is evaluated in Appendix A with the result

$$W_\mu(I) = \sqrt{2H_0(I) - 1} \times \left[\frac{\cosh\{\mu \arccos[-1/\sqrt{2H_0(I)}]\}}{\sinh \pi \mu} - \frac{1}{\pi \mu} \right]. \quad (2.20)$$

We note that the $\operatorname{sgn}(\psi)$ term of Eq. (2.19) just cancels the term $-(1/\pi\mu)$ in Eq. (2.20).

III. CLASSICAL POINCARÉ MAPS

The investigation of the dynamics is greatly simplified by a reduction of the equations of motion to a map. A straightforward way to achieve this is to discretize time in units of the period of the external field, $\Delta t = 2\pi/\omega$. The resulting map is called a stroboscopic map. Another often more useful way is to discretize time in units of actual molecular vibration periods. The resulting map is strongly characteristic of the particular molecular dynamics and is called "Morse map."

A. Stroboscopic map

The stroboscopic map at discrete times $t_n = 2\pi n/\omega$ is particularly useful if the period $2\pi/\omega$ of the external field is larger than the periods of the molecular vibrations to be investigated, which is only possible is $\omega_0 < \Omega_0$, i.e., if $\omega < 1$. Then primary resonances between the external field and the unperturbed molecular vibrations at scaled frequencies $\Omega(I) = \partial H_0^</\partial I = 1 - I$ occur for $p\omega = 1 - I$ when p photons excite one molecular phonon. For $\omega \geq 1$ primary resonances occur for $\omega = m(1 - I)$ when one photon excites m molecular phonons.

The map is obtained by solving the equations of motion

$$\dot{I} = \frac{2g}{\omega} \sum_{m=1}^{\infty} m W_m(I) \cos m \theta \sin \omega t, \quad (3.1)$$

$$\dot{\theta} = 1 - I - \frac{2g}{\omega} \sum_{m=1}^{\infty} \frac{\partial W_m(I)}{\partial I} \sin m \theta \sin \omega t$$

for one period $0 \leq t \leq 2\pi/\omega$.

A numerical example is shown in Fig. 2 where the Poincaré surface of section (θ, I) for $\omega t_n = 2\pi n$ is shown, using as coordinate $H_0(I)$, the energy of the free molecule. The parameters chosen are $\omega = 1.0$, $g = 0.01$. The primary resonances with $m = 1, 2$ are clearly visible at $H_0 \approx 0, \frac{3}{8}$, respectively. Also visible are the usual higher-order resonances, e.g., for $m = \frac{3}{2}$ at $H_0 \approx \frac{5}{18}$ or for $m = \frac{4}{3}$ at $H_0 \approx \frac{7}{32}$; Kolmogorov-Arnold-Moser (KAM) curves; and the chaotic region surrounding the $m = 2$ resonance.

B. Morse map

In order to define the Morse map we first extend the phase space by introducing the action N and the angle variable φ of the external field.¹⁴ The new Hamiltonian may then be written as

$$\hat{H}(I, N, \theta, \varphi) = H_0(I) - \frac{g}{\omega} p(I, \theta) \sin \varphi + \frac{g^2}{2\omega^2} \sin^2 \varphi + \omega N. \quad (3.2)$$

It now describes an autonomous dynamical system of two degrees of freedom. The Morse map is defined as the map induced by this Hamiltonian on the Poincaré surface of section defined by $\hat{H} = 0$, $\theta = \pi$, $\dot{\theta} > 0$. The Hamiltonian (2.12) is reobtained if φ is eliminated from Eq. (3.2) by inserting the solution of the equation of motion $\dot{\varphi} = \omega$. The origin of N in Eq. (3.2) may be chosen arbitrarily and we shall fix it by demanding that $\hat{H} = 0$ for the initial state of the system, which implies $\hat{H} = 0$ for all times. Then the total energy

$$E(t) = H(I(t), \theta(t), t) = -\omega N(t) \quad (3.3)$$

is described by $N(t)$.

As the next step we define a new molecular time coordinate \tilde{t} using the molecular oscillations as a clock.¹⁴ The pointer of this clock then is the angle $\theta = \tilde{t} \pmod{2\pi}$. The translations in the molecular time coordinate \tilde{t} are generated by a new Hamiltonian

$$\tilde{H}(N, \varphi, \tilde{t}) = -I(N, \varphi, \tilde{t}), \quad (3.4)$$

which expresses the fact the action variable I is canonically conjugate to θ . The action I as a function of N, φ, \tilde{t} is implicitly defined by the condition

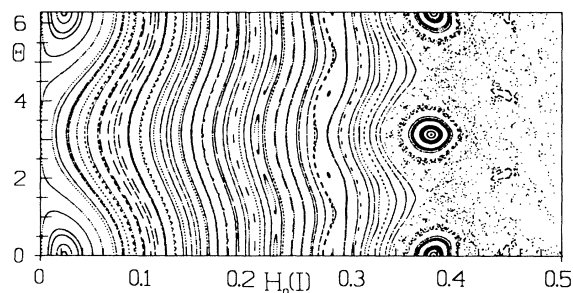


FIG. 2. Poincaré surface of section of the stroboscopic map (for $\omega = 1.0$, $g = 0.01$).

$$\hat{H}(I, N, \theta, \varphi) = 0. \quad (3.5)$$

We may solve this equation for I iteratively as a power series in g with the result

$$\tilde{H}(N, \varphi, \tilde{t}) = \tilde{H}_0(N) + \sum_{s=1}^{\infty} \frac{g^s}{\omega^s} \sin^s \varphi h_s(N, \tilde{t}) \quad (3.6)$$

and the first few terms

$$\tilde{H}_0(N) = -1 + \sqrt{1 + 2\omega N}, \quad (3.7)$$

$$h_1(N, \tilde{t}) = -\frac{p(1 - \sqrt{1 + 2\omega N}, \tilde{t})}{\sqrt{1 + 2\omega N}},$$

$$h_2(N, \tilde{t}) = -\frac{1}{2} \frac{p^2 + 2pp'\sqrt{1 + 2\omega N} - 1 - 2\omega N}{(1 + 2\omega N)^{3/2}}, \quad (3.8)$$

where $p' = dp(I, \theta)/dI$ at $I = 1 - \sqrt{1 + 2\omega N}$, $\theta = \tilde{t}$ and

$$p = \sqrt{1 + 2\omega N} \frac{\sqrt{-2\omega N} \sin \tilde{t}}{1 - \sqrt{-2\omega N} \cos \tilde{t}}. \quad (3.9)$$

The term with h_2 is small compared to the term with h_1 if

$$g \frac{|p + 2p'\sqrt{1 + 2\omega N} - (1 + 2\omega N)/p|}{1 + 2\omega N} \ll 1. \quad (3.10)$$

This condition roughly amounts to $g/\sqrt{1 + 2\omega N} \ll 1$ and cannot be satisfied very close to the unperturbed separatrix $-\omega N = \frac{1}{2}$. But apart from this exception and the trivial region close to $N = 0$ the validity of (3.10) may be assumed for physically reasonable cases, so that we can neglect the h_2 term. The higher-order terms will be still smaller. We are then left with the Hamiltonian

$$\tilde{H}(N, \varphi, \tilde{t}) = \tilde{H}_0(N) + \frac{g}{\omega} \sin \varphi h_1(N, \tilde{t}). \quad (3.11)$$

The Morse map is now the stroboscopic map at times $\tilde{t}_n = 2\pi(n - \frac{1}{2})$ induced by the Hamiltonian \tilde{H} . We shall use the notation $N_n = N(\tilde{t}_n)$, $\varphi_n = \varphi(\tilde{t}_n)$. The equations of motion following from \tilde{H} are

$$\frac{\partial N}{\partial \tilde{t}} = \frac{g}{\omega} \cos \varphi \frac{\sqrt{-2\omega N} \sin \tilde{t}}{1 - \sqrt{-2\omega N} \cos \tilde{t}}, \quad (3.12)$$

$$\frac{\partial \varphi}{\partial \tilde{t}} = \frac{\omega}{\sqrt{1 + 2\omega N}} + \frac{\omega}{2\sqrt{-2\omega N}} \frac{\sin \tilde{t} \sin \varphi}{(1 - \sqrt{-2\omega N} \cos \tilde{t})^2}.$$

In keeping with our earlier approximations they are solved to first order in $g/\sqrt{1 + 2\omega N}$ only. We obtain in zero order

$$N(\tilde{t}) = N_n, \quad \varphi(\tilde{t}) = \frac{\omega \tilde{t}}{\sqrt{1 + 2\omega N_n}} + \bar{\varphi}_n, \quad (3.13)$$

where $\bar{\varphi}_n$ is the phase at time $\tilde{t}_n = (\tilde{t}_n + \tilde{t}_{n+1})/2$. For the change of N from \tilde{t}_n to \tilde{t}_{n+1} we obtain to first order

$$\begin{aligned} \bar{N}_n = N_n + \frac{g}{\omega} \sqrt{-2\omega N_n} \int_{\tilde{t}_n}^{\tilde{t}_{n+1}} d\tilde{t} \cos \left[\frac{\omega \tilde{t}}{\sqrt{1 + 2\omega N_n}} + \bar{\varphi}_n \right] \\ \times \frac{\sin \tilde{t}}{1 - \sqrt{-2\omega N_n} \cos \tilde{t}}. \end{aligned} \quad (3.14)$$

From Eq. (3.14) we obtain

$$\bar{N}_n = N_n + \frac{g}{2} [f(N_n) \sin \bar{\varphi}_n + k(N_n) \cos \bar{\varphi}_n], \quad (3.15)$$

where the functions $f(N)$ and $k(N)$ are defined by the integrals

$$f(N) = -\frac{2\sqrt{-2\omega N}}{\omega} \int_0^\pi dx \sin \frac{\omega x}{\sqrt{1+2\omega N}} \times \frac{\sin x}{1-\sqrt{-2\omega N} \cos x}, \quad (3.16)$$

$$k(N) = \frac{2\sqrt{-2\omega N}}{\omega} \int_0^\pi dx \cos \left[\frac{\omega x}{\sqrt{1+2\omega N}} \right] \times \frac{\sin x}{1-\sqrt{-2\omega N} \cos x}.$$

Let us now turn to the change of φ from \tilde{t}_n to \bar{t}_n . To first

order in $g/\sqrt{1+2\omega N}$ we find

$$\bar{\varphi}_n = \varphi_n + \frac{\pi\omega}{\sqrt{1+2\omega N_n}} - \frac{\omega^2}{\sqrt{(1+2\omega N_n)^3}} \int_{-\pi}^0 [N(x) - N_n] dx - \frac{g}{\omega} \int_{-\pi}^0 dx \sin \left[\frac{\omega x}{\sqrt{1+2\omega N_n}} + \bar{\varphi}_n \right] \times \frac{\partial}{\partial N_n} \left[\frac{\sqrt{-2\omega N_n} \sin x}{1-\sqrt{-2\omega N_n} \cos x} \right], \quad (3.17)$$

where the fourth term on the right-hand side has been rewritten in a useful way. Upon partial integration of the third and fourth terms on the right-hand side we find

$$\bar{\varphi}_n = \varphi_n + \frac{\omega\pi}{\sqrt{1+2\omega N_n}} + \frac{\omega^2}{\sqrt{(1+2\omega N_n)^3}} \int_{-\pi}^0 x \frac{dN}{dx} dx - \frac{g}{\omega} \frac{\partial}{\partial N_n} \int_{-\pi}^0 dx \frac{\sqrt{-2\omega N_n} \sin x \sin(\omega x / \sqrt{1+2\omega N_n})}{1-\sqrt{-2\omega N_n} \cos x} \cos \bar{\varphi}_n - \frac{g}{\omega} \frac{\partial}{\partial N_n} \int_{-\pi}^0 dx \frac{\sqrt{-2\omega N_n} \sin x \cos(\omega x / \sqrt{1+2\omega N_n})}{1-\sqrt{-2\omega N_n} \cos x} \sin \bar{\varphi}_n - \frac{g\omega}{\sqrt{(1+2\omega N_n)^3}} \int_{-\pi}^0 dx \left[x \cos \left[\frac{\omega x}{\sqrt{1+2\omega N_n}} + \bar{\varphi}_n \right] \frac{\sqrt{-2\omega N_n} \sin x}{1-\sqrt{-2\omega N_n} \cos x} \right]. \quad (3.18)$$

The integrand of the last term on the right-hand side may be simply rewritten as $x \partial N / \partial x$ by using the equation of motion, and it is then seen that it cancels with the third term. Finally, the fourth term may be expressed as $\frac{1}{2} g f'(N_n) \cos \bar{\varphi}_n$ and similarly the fifth term can be written as $-\frac{1}{2} g k'(N_n) \sin \bar{\varphi}_n$. Using all these observations we find

$$\bar{\varphi}_n = \varphi_n \frac{\pi\omega}{\sqrt{1+2\omega N_n}} + \frac{1}{2} g [f'(N_n) \cos \bar{\varphi}_n - k'(N_n) \sin \bar{\varphi}_n]. \quad (3.19)$$

A very similar calculation gives the map $(N_{n+1}, \varphi_{n+1}) \rightarrow (N_n, \bar{\varphi}_n)$ backwards in time \tilde{t} from \tilde{t}_{n+1} to \tilde{t}_n . We obtain

$$\bar{N}_n = N_{n+1} - \frac{g}{2} [f(N_{n+1}) \sin \bar{\varphi}_n - k(N_{n+1}) \cos \bar{\varphi}_n], \quad (3.20)$$

$$\bar{\varphi}_n = \varphi_{n+1} - \frac{\pi\omega}{\sqrt{1+2\omega N_{n+1}}} - \frac{g}{2} [f'(N_{n+1}) \cos \bar{\varphi}_n + k'(N_{n+1}) \sin \bar{\varphi}_n].$$

Combining the maps from $\tilde{t}_n \rightarrow \bar{t}_n \rightarrow \tilde{t}_{n+1}$ we obtain finally

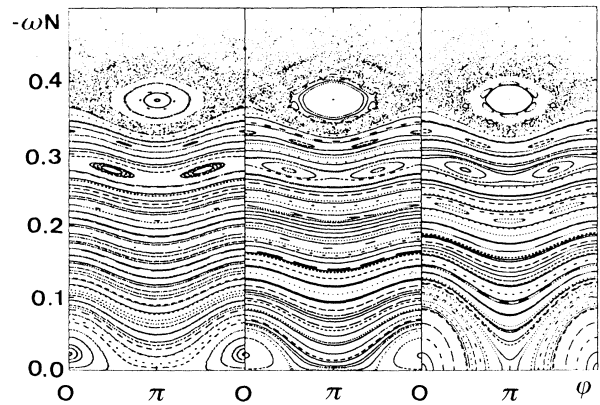


FIG. 3. Poincaré cross section of the full dynamics, the refined Morse map, and the Morse map (from left to right, for $\omega = 1.0, g = 0.01$).

$$\begin{aligned}
\varphi_{n+1} &= \varphi_n + \frac{\pi\omega}{\sqrt{1+2\omega N_n}} + \frac{\pi\omega}{\sqrt{1+2\omega N_{n+1}}} \\
&+ \frac{g}{2} \cos \bar{\varphi}_n [f'(N_n) + f'(N_{n+1})] \\
&- \frac{g}{2} \sin \bar{\varphi}_n [k'(N_n) - k'(N_{n+1})], \\
N_{n+1} &= N_n + \frac{g}{2} \sin \bar{\varphi}_n [f(N_n) + f(N_{n+1})] \\
&+ \frac{g}{2} \cos \bar{\varphi}_n [k(N_n) - k(N_{n+1})],
\end{aligned} \tag{3.21}$$

where $\bar{\varphi}_n$ is determined implicitly by Eq. (3.19). It is useful to reformulate this map, in particular with a view to its later quantization, by a convolution of four basic steps: (1) free propagation for $\tilde{t}_n \leq \tilde{t} \leq \tilde{t}_n$; (2) a first instantaneous kick; (3) a second different instantaneous kick; (4) free propagation for $\tilde{t}_n \leq \tilde{t} \leq \tilde{t}_{n+1}$. The four maps corre-

sponding to these four steps are

$$\begin{aligned}
(1) \quad \varphi' &= \frac{\pi\omega}{\sqrt{1+2\omega N_n}} + \varphi_n, \quad N'_n = N_n; \\
(2) \quad \bar{\varphi}_n &= \varphi' + \frac{g}{2} f'(N'_n) \cos \bar{\varphi}_n + \frac{g}{2} k'(N'_n) \sin \bar{\varphi}_n, \\
\bar{N}_n &= N'_n + \frac{g}{2} f(N'_n) \sin \bar{\varphi}_n + \frac{g}{2} k(N'_n) \cos \bar{\varphi}_n; \\
(3) \quad \bar{\varphi}'_n &= \bar{\varphi}_n + \frac{g}{2} f'(\bar{N}'_n) \cos \bar{\varphi}_n - \frac{g}{2} k'(\bar{N}'_n) \sin \bar{\varphi}_n, \\
\bar{N}'_n &= \bar{N}_n + \frac{g}{2} f(\bar{N}'_n) \sin \bar{\varphi}_n - \frac{g}{2} k(\bar{N}'_n) \cos \bar{\varphi}_n; \\
(4) \quad \varphi_{n+1} &= \frac{\pi\omega}{\sqrt{1+2\omega N_{n+1}}} + \bar{\varphi}'_n, \quad N_{n+1} = \bar{N}'_n
\end{aligned} \tag{3.22}$$

and can be described by the Hamiltonian

$$\begin{aligned}
H_{\text{eff}} &= -1 + \sqrt{1+2\omega N} + \frac{g}{2} \sum_{n=-\infty}^{+\infty} \delta(\tilde{t} - 2\pi n) \{ [f(N(\tilde{t} - \epsilon)) + f(N(\tilde{t} + \epsilon))] \cos \varphi(\tilde{t}) \\
&+ [k(N(\tilde{t} - \epsilon)) - k(N(\tilde{t} + \epsilon))] \sin \varphi(\tilde{t}) \},
\end{aligned} \tag{3.23}$$

where $\epsilon \rightarrow +0$.

Now merely the task is left to evaluate the integrals (3.16). Using the Fourier expansion (2.14) we obtain

$$\begin{aligned}
f(N) &= \frac{-4}{\sqrt{1+2\omega N}} \sum_{m=1}^{\infty} \left[\frac{1 - \sqrt{1+2\omega N}}{1 + \sqrt{1+2\omega N}} \right]^{m/2} \frac{\sin(\omega/\sqrt{1+2\omega N} - m)\pi}{\omega^2/(1+2\omega N) - m^2}, \\
k(N) &= \frac{-4}{\sqrt{1+2\omega N}} \sum_{m=1}^{\infty} m \left[\frac{1 - \sqrt{1+2\omega N}}{1 + \sqrt{1+2\omega N}} \right]^m \frac{1 - \cos(\omega/\sqrt{1+2\omega N} - m)\pi}{\omega^2/(1+2\omega N) - m^2}.
\end{aligned} \tag{3.24}$$

The sums are dominated by the terms where $m \simeq \omega/\sqrt{1+2\omega N}$ and may therefore be approximated by

$$\begin{aligned}
f(N) &\simeq \frac{-2\pi}{\omega} \left[\frac{1 - \sqrt{1+2\omega N}}{1 + \sqrt{1+2\omega N}} \right]^{\omega/2\sqrt{1+2\omega N}}, \\
k(N) &\simeq 0.
\end{aligned} \tag{3.25}$$

Our map (3.21) and (3.19) simplifies considerably by setting $k(N) = 0$. This final result, together with the function $f(N)$, was reported in our earlier paper.⁹ It was called “refined Morse map.” In Appendix B we give an alternative rather short direct derivation of its Hamiltonian (3.23). A simpler but more restricted version is obtained by approximating the function $f(N)$ further for $\omega/\sqrt{1+2\omega N} \gg 1$, which holds for highly excited molecular states. However, it must be kept in mind that we still have to satisfy $g\omega/\sqrt{1+2\omega N} \ll 1$ in order to validate our expansion in this small parameter. We may then set

$$f(N) \simeq -\frac{2\pi}{\omega} e^{-\omega} \tag{3.26}$$

and the map (3.21) and (3.19) becomes simply

$$\begin{aligned}
\varphi_{n+1} &= \varphi_n + \frac{\pi\omega}{\sqrt{1+2\omega N_n}} + \frac{\pi\omega}{\sqrt{1+2\omega N_{n+1}}}, \\
N_{n+1} &= N_n - \frac{2\pi g}{\omega} e^{-\omega} \sin \left[\varphi_n + \frac{\pi\omega}{\sqrt{1+2\omega N_n}} \right],
\end{aligned} \tag{3.27}$$

which was called “Morse map” in.⁹ In Fig. 3 we give a comparison of the Poincaré map computed numerically from the full Hamiltonian flow, the refined Morse map, Eqs. (3.21) and (3.19); Eq. (3.25); and the simplified Morse map, Eq. (3.27) for $\omega = 1$, $g = 0.01$. It can be seen that the refined Morse map faithfully reproduces the invariant manifolds of the numerically exact map, and that the simple Morse map works well except for the manifolds at small energies. The breakdown of the validity of the maps near the dissociation threshold $\omega N = -\frac{1}{2}$ is not apparent in these figures as this region is already in the fully chaotic domain.

The Morse map⁹ is similar to the “Kepler map”^{3,15} describing Rydberg atoms in strong microwave fields along similar lines.¹⁴ Recently it has also been obtained in Ref. 16.

C. Dissociation probability

In order to use the refined Morse map to compute the dissociation probability of the molecule for a fixed (dimensionless) interaction time T or a fixed number of iterations of the map and a given initial energy of the molecule one proceeds as follows. The computation is done for many ($Z \gg 1$) initial states at the same energy $E_0 = -\omega N_0$ and randomly distributed phases φ_0 . In order to apply the map for the step $n \rightarrow n+1$ one first solves the transcendental equation (3.19) for $\bar{\varphi}_n$, which has a unique solution if $gf'(N_n) < 2$, then the transcendental equation (3.21) is solved for N_{n+1} and then Eq. (3.21) can be solved for φ_{n+1} . The solution of two transcendental equations is therefore necessary for each step. Each point having reached the value $-\omega N_{n+1} > \frac{1}{2}$ is dropped from the further calculation as the corresponding molecule is dissociated. The dissociation probability $P(n)$ at a fixed number of iterations is therefore given by

$$P(n) = 1 - \frac{Z(n)}{Z}, \quad (3.28)$$

where $Z(n)$ is the number of points left after n interactions. In order to determine the dissociation probability $\bar{P}(T)$ for a fixed value of the (dimensionless) physical time $\omega t = \omega T$ one has to perform the same calculation, but in addition one has to keep track, for each system point j , of its value for $\omega t_n = \varphi_n = \varphi_n^{(j)}$ not taken modulo 2π .

For each system point the computation must be carried out until either its $-\omega N$ value exceeds $\frac{1}{2}$, in which case it is counted as dissociated and omitted, or its φ_n value exceeds ωT , in which case it is counted as not dissociated and the value of a number $\bar{Z}(T)$ increased by 1. Then

$$\bar{P}(T) = 1 - \bar{Z}(T)/Z. \quad (3.29)$$

D. Estimates obtained from the Morse map

The Morse map derived in Sec. III C lends itself to a number of simple estimates which we now give.

(i) Primary resonances with integer winding number m , where m field cycles coincide with one molecular cycle, occur for molecular energies

$$E_m = -\omega N_m = \frac{1}{2} \left[1 - \frac{\omega^2}{m^2} \right]. \quad (3.30)$$

The corresponding elliptic islands for $m=1,2$ are clearly visible in Fig. 3. Also visible there are the resonances at $m = \frac{3}{2}$ ($\frac{5}{3}$) when 3 (5) field cycles coincide with 2 (3) molecular cycles.

(ii) Near a resonance the map can be approximated locally by the standard map^{17,18}

$$\begin{aligned} \varphi_{n+1} &= \varphi_n - T_m \delta N_{n+1}, \\ \delta N_{n+1} &= \delta N_n + k_m \sin \varphi_n, \end{aligned} \quad (3.31)$$

where $\delta N_n = N_n + [(1 - \omega^2/m^2)/2\omega]$ and

$$T_m = \frac{2\pi m^3}{\omega}, \quad k_m = -\frac{2\pi g}{\omega} \left[\frac{m-\omega}{m+\omega} \right]^{m/2} (-1)^m. \quad (3.32)$$

The transition to global chaos at the resonance m occurs when the last KAM torus separating it from the resonance $m+1$ is destroyed.¹⁸ This breakup can be estimated by the use of the local standard map and occurs there for $K_m \equiv |k_m T_m| > 0.97\dots$ ¹⁹ The threshold to global chaos at the resonance m is therefore obtained at the field amplitude

$$|g| > g_c(m) = 0.97 \frac{\omega^2}{4\pi^2 m^3} \left[\frac{m+\omega}{m-\omega} \right]^{m/2}. \quad (3.33)$$

The KAM torus between the resonances m and $m+1$ to break up last is expected to have the winding number $\mu = m + \gamma^{-2}$ (Ref. 19) where $\gamma = (1 + \sqrt{5})/2$ is the golden mean. Its average energy is at

$$E_m^c = -\omega N_m^c \simeq \frac{1}{2} \left[1 - \frac{\omega^2}{(m + \gamma^{-2})^2} \right]. \quad (3.34)$$

Hence Eq. (3.34) with m the largest integer with $g_c(m) > |g|$ specifies the molecular energy where chaos sets in.

(iii) The flux of action ΔW_m per iteration passing through the broken KAM torus (Cantor set) at energy E_m^c can be estimated as^{20,21}

$$\Delta W_m \simeq 0.37 \frac{\omega}{\pi m^3} \left[\ln \frac{|g|}{g_c(m)} \right]^{3.0117\dots} \quad (3.35)$$

provided the expression in large parentheses is small compared to 1.

(iv) The local diffusion constant of the energy in the fully chaotic domain is estimated from the local standard map as

$$D_m = \lim_{n \rightarrow \infty} \frac{(N_n - N_0)^2}{n} \simeq \frac{2\pi^2 g^2}{\omega^2} \left[\frac{m-\omega}{m+\omega} \right]^m F(K_m), \quad (3.36)$$

where $F(K_m)$ is a known function^{22,18} of order 1 which would exactly equal 1 if phase correlations between subsequent kicking periods of the map could be neglected.

IV. QUANTIZATION

A. Quantization of the Morse map

The molecular dynamics is quantized by imposing the commutation relation

$$[p, x] = -i\hbar. \quad (4.1)$$

Then the familiar energy levels of the Morse oscillator are obtained,

$$E_\nu = I_\nu - \frac{1}{2} I_\nu^2, \quad (4.2)$$

with quantum numbers $I_\nu = \hbar(\nu + \frac{1}{2})$. The corresponding eigenstates are called χ_ν . The dimensionless parameter \hbar in our present units is really the dimensionless constant $(\hbar\Omega_0/2D) \ll 1$, which equals the inverse of the number of bound states supported by the Morse potential.

constant $(\hbar\Omega_0/2D) \ll 1$, which equals the inverse of the number of bound states supported by the Morse potential.

We can also quantize the Morse map, which is symplectic, with the canonical pair of variables N, φ . Then we impose

$$[N, \varphi] = -i\hbar \quad (4.3)$$

and choose, with an arbitrary κ in $0 \leq \kappa < 1$,

$$N = -i\hbar \frac{\partial}{\partial \varphi} - \hbar\kappa \quad (4.4)$$

with eigenstates

$$N|l\rangle = \hbar(-l - \kappa)|l\rangle, \quad (4.5)$$

where l is integer. Let us suppose that the initial state is a direct product $\Psi = \chi_{v_0} \psi_{l_0}$. In order to fix l_0 and κ we satisfy the condition (3.5) in the form¹⁴

$$\langle \Psi | \hat{H}(I, N, \theta, \varphi) | \Psi \rangle = 0, \quad (4.6)$$

which yields

$$l_0 + \kappa_0 = E_{v_0} / \hbar\omega, \quad (4.7)$$

i.e., l_0 and κ_0 are the integer and fractional part of the right-hand side, respectively. Physically, the integer l_0 gives the number of photons needed to excite the molecule from its ground state at $E_0 \approx \hbar/2$ to the state at E_{v_0} . The l_0 interval corresponding to the bound subspace is

$$\frac{1}{2\omega} \leq l_0 \leq \frac{1}{2\hbar\omega}. \quad (4.8)$$

The unbound subspace corresponds to $l_0 \geq 1/2\hbar\omega + 1$ while all values $l_0 \leq 1/2\omega - 1$ are unphysical and should have zero probability.

Having determined the initial state for the map the further evolution of this state is described by the quantized map

$$|\psi_{n+1}\rangle = U|\psi_n\rangle. \quad (4.9)$$

The operator U is most easily constructed using the decomposition (3.22) of the map. Steps (1) and (4) are described by the unitary operator $\exp[-(i\pi/\hbar)\tilde{H}_0(N)]$, where \tilde{H}_0 was defined in Eq. (3.7). The symmetric kick in steps (3) and (4) is described by

$$K(N, \varphi) = \exp\left[-\frac{ig}{2\hbar}[f(N)\cos\varphi + \cos\varphi f(N)]\right]. \quad (4.10)$$

Its elements $K_{ll'}$ must be determined numerically (cf. Appendix C). In the limit where the simplified Morse map applies (cf. C2) the matrix $K_{ll'}$ is known in closed form

$$K_{ll'} = (-i)^{l-l'} J_{l-l'} \left[-\frac{2\pi g}{\hbar\omega} e^{-\omega} \right], \quad (4.11)$$

where the J_l are the Bessel functions. The fact that K describes the net effect of the total interaction with the external field over a molecular period is a big advantage of the present method. In particular excitation into the

unbound subspace with subsequent deexcitation back to the bound subspace within the same molecular period is fully contained in K , provided the Morse map is extended to the unbound subspace. This is done in Appendix B by using the results of Sec. III C. The complete operator U then reads

$$U = e^{-i(\pi/\hbar)\tilde{H}_0} P K e^{-i(\pi/\hbar)\tilde{H}_0}, \quad (4.12)$$

where

$$P_{ll'} = \Theta \left[\left[\frac{1}{2\hbar\omega} \right] - l \right] \delta_{ll'} \quad (4.13)$$

is the projector on the bound subspace and Θ is the step function. It describes the fact that the probability amplitude for dissociation after each kick is given by the component of the wave function in the unbound subspace.³ Thus deexcitation processes occurring for time intervals longer than the preceding molecular period (but *not* those occurring for shorter time intervals) are neglected.

The dissociation probability after n iterations of the map is given by

$$P(n) = 1 - \sum_{l=1/2\omega}^{1/2\hbar\omega} |\langle l | \psi_n \rangle|^2, \quad (4.14)$$

where $|\psi_n\rangle = U^n |\psi_0\rangle$. There is as yet no really good general way to convert the result (4.14) back to the physical time t . The best one can do at present is to convert to real time via the n -dependent mean molecular frequency $2\pi/\Delta t$ for the wave function $|\psi_n\rangle$. Classically one may approximate, e.g.,

$$\frac{2\omega}{\Delta t} \approx \frac{\sqrt{1+2\omega N_n}}{2\omega} + \frac{\sqrt{1+2\omega N_{n-1}}}{2\omega} \quad (4.15)$$

and use this expression to form the n -dependent expectation value

$$\omega \left\langle \frac{2\pi}{\Delta t} \right\rangle_n = \frac{\langle \psi_n | \sqrt{1+2\omega N} | \psi_n \rangle}{2\langle \psi_n | \psi_n \rangle} + \frac{\langle \psi_{n-1} | \sqrt{1+2\omega N} | \psi_{n-1} \rangle}{2\langle \psi_{n-1} | \psi_{n-1} \rangle}. \quad (4.16)$$

Then one may define the time $t = t(n)$ with $\Delta t = t(n) - t(n-1)$ by

$$\frac{2\pi}{\Delta t} = \left\langle \frac{2\pi}{\Delta t} \right\rangle_n, \quad (4.17)$$

$$t(n) = \sum_{k=1}^n \frac{2\pi}{\left\langle \frac{2\pi}{\Delta t} \right\rangle_k},$$

and one can calculate

$$\bar{P}(t) = P(n_{\max}(t)) \quad (4.18)$$

by computing $P(n)$, $t(n)$ until $t(n_{\max} + 1) > t$. This procedure can be expected to work the better the more localized the wave function $\langle l | \psi_n \rangle$ remains with respect to the quantum number l .

B. Quantum effects described by the Morse map

The Morse map allows to make a number of predictions on the quantum level, which parallel the predictions on the classical level made in Sec. III D.

(i) The primary resonances with winding number m quantum mechanically correspond to one-photon- m -phonon resonances. The external field should therefore mix initial states of energy $E_{v_0} \simeq E_m = -\omega N_m$ with states lying a photon higher or lower and such states should therefore dissociate with a resonantly enhanced probability or should be resonantly stabilized. A different way to phrase the resonant stabilization of states near the one-photon resonances makes use of the notion of “scars,” i.e., the constructive interference of wave functions in the classically chaotic domain on short (unstable) periodic orbits.²³ Hyperbolic periodic orbits with winding number m occur in the classical map at energies $E \simeq E_m$. In phase space the quasiprobability distributions (e.g., the Wigner distribution or the Husimi distribution) of scarred wave functions are known to display enhancement also on parts of the stable and (or) unstable manifolds of the periodic orbits.^{24,25} These manifolds surround the eventually coexisting elliptic periodic orbits at the same winding number. Hence resonantly stabilized or scarred states may be found slightly above or below the energies $E_{v_0} \simeq E_m$. For hydrogen atoms in strong microwave field this was discussed in Ref. 26.

(ii) Initial states with energies below the classical chaos border (3.34) will remain rather localized in energy as the quasiprobability distribution of wave functions are spread out along the KAM curves but fall off in the transversal direction on a characteristic length scale (in l) given by the absolute value of the argument of the Bessel function in Eq. (4.11). For $|l-l'|$ larger than this value the kick operator K goes to zero rapidly. Hence the prediction that excitation to high energies are not observed for such initial states.

(iii) Even after breakup of a KAM torus the remaining “Cantorus” can continue to form an effective barrier and to localize wave functions.^{27,28} A simple estimate of how long a Cantorus may be active in this way results from the comparison of ΔW_m , Eq. (3.35), with \hbar ,^{20,29} i.e., one predicts a border between a regular, localized regime of initial states which are not excited to high energies and an irregular regime where excitation to high energies is not forbidden by any effective barriers in phase space. A heuristic estimate for this threshold is provided by the condition.^{20,29}

$$\Delta W_m > \hbar \quad (4.19)$$

for the Cantorus no longer being active as a barrier. One arrives at this comparison by noting that it is impossible to compress a quantum state in phase space on an area smaller than $\Delta p \Delta q = \pi \hbar / 2$ where q and p are conjugate variables.

(iv) In the regime where $\Delta W_m > \hbar$ is satisfied it would seem that quantum-mechanical wave functions could spread out uninhibited in analogy to the uninhibited classical diffusion process occurring in this regime. However,

due to a process of “dynamical localization”^{3,30–34} similar to Anderson localization of waves in disordered systems,³¹ an uninhibited spreading of wave functions is, in fact, not predicted. Instead a destructive interference of the many different multiple-photon transition amplitudes corresponding to the multitude of classical diffusion paths is predicted to occur for final states at energies separated by more than a localization length $\hbar \omega l'_A$ from the initial energy. The localization length l'_A was shown to be equal, apart from a factor α of the order of 1, to the classical diffusion constant (3.36) expressed in units of the quantum number l (Ref. 34).

$$l_A = \alpha D^{(l)} = \alpha \frac{2\pi^2 g^2}{(\hbar \omega)^2} \left(\frac{m-\omega}{m+\omega} \right)^m F(K_m). \quad (4.20)$$

For an exactly solvable model $\alpha = \frac{1}{2}$ was found in Ref. 29. In the ideal case of complete exponential dynamical localization the eigenfunctions of the map U would behave like

$$|\varphi_l|^2 \sim \exp \left[-\frac{2|l-l_0|}{l'_A} \right]. \quad (4.21)$$

However, l'_A itself fluctuates, in general, from state to state, and the exponential decay of the average of $|\varphi_l|^2$ over the initial state occurs therefore on a length²⁹

$$l_A \simeq 2l'_A = 2\alpha D^{(l)} \simeq D^{(l)}. \quad (4.22)$$

In the case of the Morse map complete dynamical localization cannot be expected to occur due to a “finite-size effect,” i.e., the fact that only a finite number of bound states is supported by the Morse potential. Hence the destructive interference of multiple-photon transition amplitudes is not complete and dynamical localization reduces the dissociation rate and the excitation rate to high energies below the classical value without extinguishing dissociation completely. If the initial state lies near the dissociation threshold within a localization length l_A no quantum-mechanical inhibition of dissociation by localization is predicted to occur.

V. NUMERICAL RESULTS

A. Time-dependent expectation values

Using the Morse map in its classical and its quantum-mechanical form it is possible to calculate time-dependent expectation values like the average molecular energy $\langle E \rangle$ and the dissociation probability P . Quantum mechanically we have to evaluate the expressions (4.14) for $P(n)$ and

$$\langle E(n) \rangle = \sum_l \hbar \omega (l + \kappa) |\langle l | \psi_n \rangle|^2 / [1 - P(n)] \quad (5.1)$$

for the average energy and convert n to the physical time $t(n)$ by the use of Eq. (4.17). The corresponding classical expressions are given, respectively, by Eq. (3.29) and

$$\langle E(t) \rangle = \frac{1}{\bar{Z}(t)} \sum_{i=1}^{\bar{Z}(t)} (-\omega N_i), \quad (5.2)$$

where the sum is extended over the same $\bar{Z}(t)$ particles which contribute to Eq. (3.29) and $-\omega N_i$ is their energy when their time $t_n = \varphi_n^{(j)}$ first exceeds t . The classical and quantum-mechanical results for the Morse map are compared, in the following, with results of a direct numerical solution of the classical equations of motion and with a completely independent approach to the quantum-mechanical problem which comes from a direct numerical solution of the Schrödinger equation. We shall present this work in a separate paper,³⁵ but shall use some of its results here for the sake of comparison.

In Figs. 4–6 we consider the excitation of the molecule from its ground state and choose the parameters $\hbar=0.0419$, $\omega=0.945$, and choose increasing values of g , $g=0.02$, 0.07 , and 0.14 , respectively. In the classical case the equations of motion are solved directly for an ensemble of initial conditions with fixed value of $H_0(I)$ (equal to $\hbar/2$ for Figs. 4–6) and equidistributed values of the two phase variables θ and φ . A second calculation was performed with the refined Morse map, with the initial value for N chosen to satisfy the condition $\langle \hat{H} \rangle = 0$, where $\langle \rangle$ denotes the average over the initial ensemble of the first calculation. The comparison of both calculations is seen in the upper part of Figs. 4–6.

In the quantum case the Schrödinger equation was solved directly³⁵ with a molecular eigenstate $|\psi_{\text{mol}}\rangle$ (the ground state in Figs. 4–6) as the initial state. A corresponding calculation was performed with the quantized refined Morse map. The initial state $|\psi_0\rangle$ for the Morse map was fixed in this case by assuming the total wave function $|\chi_{\text{tot}}\rangle$ of field and molecule to factorize initially $|\chi_{\text{tot}}\rangle = |\psi_{\text{mol}}\rangle \otimes |\psi_0\rangle$ into the eigenstate of $H_0(I)$ and the eigenstate of ωN and imposing the condition

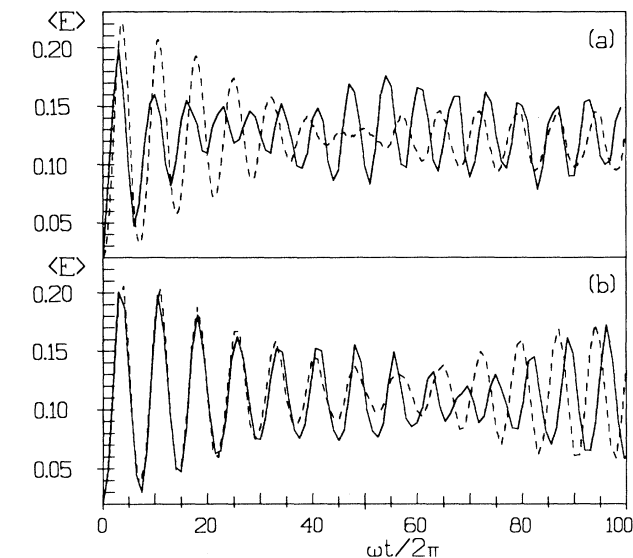


FIG. 5. The same as in Fig. 4 for $g=0.07$.

$\langle \chi_{\text{tot}} | \hat{H} | \chi_{\text{tot}} \rangle = 0$. This condition fixes $|\psi_0\rangle = |l_0\rangle$ with $\hbar\omega(l_0 + \kappa_0) = \langle \psi_{\text{mol}} | H_0(I) | \psi_{\text{mol}} \rangle$ according to (4.5). The comparison of the results of both quantum calculations is shown in the lower part of Figs. 4–6.

The parameters of Fig. 4 were chosen to permit also a comparison with the results of Walker and Preston.⁴ The molecule is excited at most to the vibrational state $\nu=3$. The classical and quantum Morse map are seen to give good approximations in this case to the results of a fuller calculation, which, in the quantum case require computation times which are orders of magnitudes larger. In Fig. 5 the external field is stronger, the molecule is now excit-

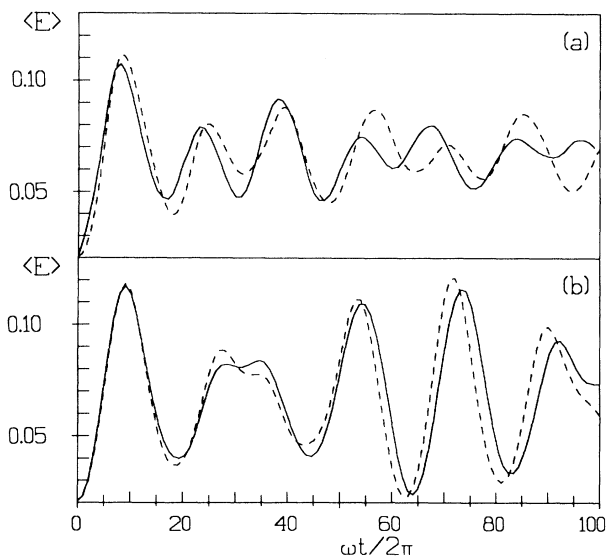


FIG. 4. $\langle E \rangle$ as a function of $\omega t / 2\pi$, (a) classical and (b) quantum results. The dashed line in (a) is the result of a direct solution of the classical equations of motion and in (b) of an approximate solution of the Schrödinger equation (Ref. 35). The parameters are $\hbar=0.0419$, $\omega=0.945$, $g=0.02$.

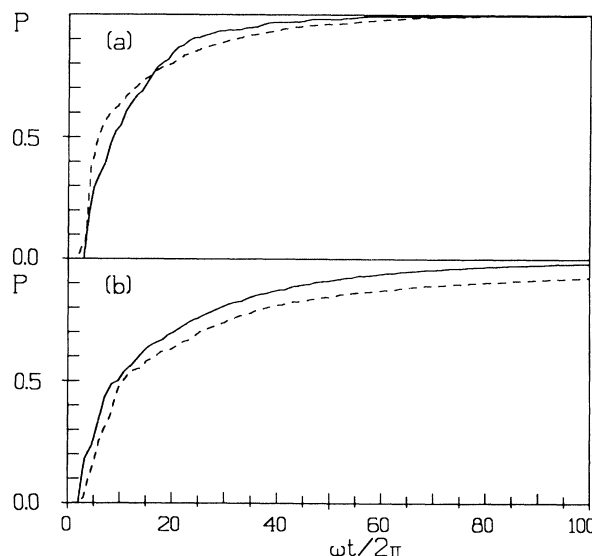


FIG. 6. Dissociation probability P as a function of $\omega t / 2\pi$ for $g=0.14$.

ed from the ground state up to $\nu \approx 5$. The results obtained from the map describe amplitude and frequency of the Rabi-type oscillations qualitatively correctly, however, the detailed time dependence is not reproduced faithfully in phase and amplitude, which is hardly surprising in view of the fact that the molecular eigenstates $|\nu\rangle$ have been replaced by effective photon states $|l\rangle$. In Fig. 6 the dissociation probability from the ground state is given for $g=0.14$. The classical chaos border obtained from Eq. (3.33) is at $g=0.16$, consistent with the fact that $P=0$ for Figs. 4 and 5. Yet it is somewhat too high, even quantum mechanically, because it would predict $P=0$ even in Fig. 6. The quantum result and the classical result in Fig. 6 are very similar to each other. Again the map is seen to reproduce the time dependence qualitatively well.

B. Floquet states

The eigenstates of the quantum map U are called Floquet states $|\lambda\rangle$

$$U|\lambda\rangle = b_\lambda |\lambda\rangle. \quad (5.3)$$

These eigenstates and their eigenvalues have been computed for the parameter values $\hbar=0.01$, $\omega=1.0$, $g=0.01$ and have been ordered and labeled by the integer λ according to their mean energy $\langle E(\lambda) \rangle = \sum_l \hbar\omega(l+\kappa) |\langle l|\lambda\rangle|^2$. In Fig. 7 we plot $|\langle l|\lambda\rangle|^2$ over an (l, λ) plane for those states whose mean energy falls into the bound subrange $0 \leq E(\lambda) \leq \frac{1}{2}$. The localization of all states is apparent from this diagram. The states near the $m=1$ resonance for the small λ values are broadened, as one would expect from the classical phase-space structure in Fig. 3. [It should be recalled that the probabilities $|\langle l|\lambda\rangle|^2$ correspond to the projections of the classical invariant manifolds labeled by λ onto the $-\omega N = \hbar\omega(l+\kappa)$ axis.] Also not unexpectedly states near the dissociation energy, i.e., at the large λ values, extend to the unbound energy range. However, quite remarkably, all Floquet states in the classically chaotic region (starting at about $\lambda=33$) are localized despite the fact that their corresponding classical invariant manifold, the chaotic domain, is extended. This can be understood as a consequence of dynamical localization described in

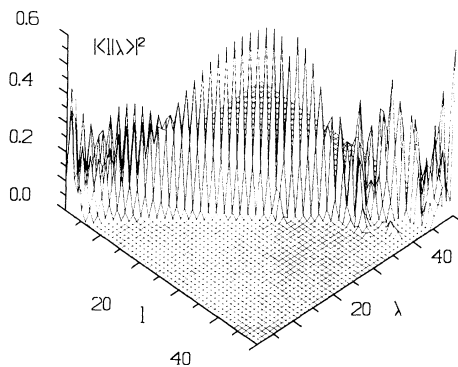


FIG. 7. Eigenstates $|\langle l|\lambda\rangle|^2$ of the quantized refined Morse map (here and in the following for $\omega=1$, $g=0.01$, $\hbar=0.01$).

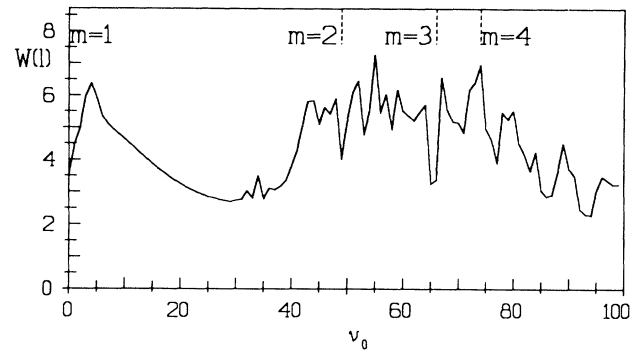


FIG. 8. Width function $W(l)$ vs the vibrational quantum number ν_0 corresponding to l .

Sec. IV B. An objective measure for the effective number of states $|\lambda\rangle$ necessary to represent a state $|l\rangle$ is the width function $W(l) = \exp(s(l))$ with $s(l) = -\sum_\lambda |\langle l|\lambda\rangle|^2 \ln |\langle l|\lambda\rangle|^2$, which was introduced in Ref. 36. The width function corresponding to the states of Fig. 7 is shown in Fig. 8 as a function of the vibrational quantum number ν of the molecular state where $\hbar\omega(l+\kappa) = -\frac{1}{2}[\hbar(\nu+\frac{1}{2})-1]^2 + \frac{1}{2}$. Conspicuous features of this result are the enhancement of the width near the first primary resonance at $m=1$, a rather smooth and systematic drop and reenhancement near around the resonance $m=2$ where classical chaos sets in (cf below), and a much more erratic variation of the width function in the classically chaotic domain, with local maxima at $m=3$ and 4. The systematic decrease of the average of W towards the dissociation border by a factor of $\frac{1}{2}$ can be explained by the extension of the states $|l\rangle$ in the $|\lambda\rangle$ -basis to $|\lambda\rangle$ states in the unbound energy range, which is projected out in U .

The eigenvalues b_λ of U are shown in Fig. 9. Most ei-

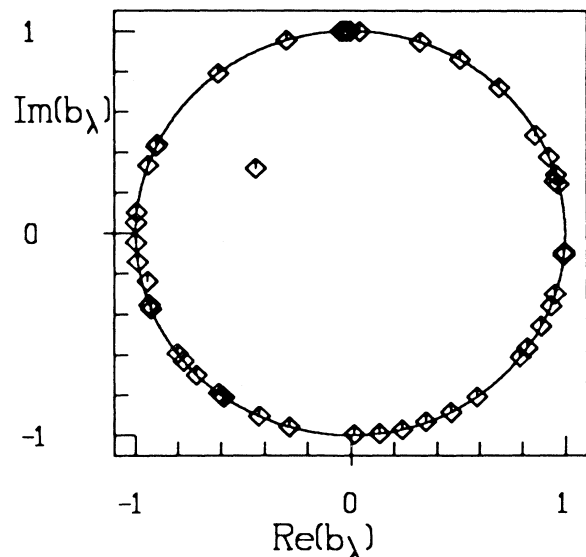


FIG. 9. Eigenvalues of the quantized refined Morse map in the complex plane.

genvalues lie practically on the unit circle, but some are displaced visibly and a single one even strongly inside the unit circle, due to the decay of the eigenstates close to the dissociation energy. The mathematical reason is, of course, again the appearance of the projector P on the bound subspace in the definition of U .

C. Dissociation probability as a function of the initial state

As our next result we discuss the dissociation probability for a given molecular time (here fixed at 100 passages through the nuclear distance minimum). In Fig. 10 we plot as a function of the initial molecular energy $H = -\omega N$ the classical dissociation probability (upper curve) and the corresponding quantum result (lower curve) and compare them with the corresponding classical phase-space structure (lower part of the diagram corresponding to Fig. 1). The classical dissociation is seen to begin precisely at the classical chaos border whose analytical estimate, following from (3.33) and (3.34) by eliminating m , is given as B_C . The quantum result gives a higher dissociation threshold which is well explained by Cantorus localization derived from (4.19) and (3.35) with $m = 2$. The position of the Cantorus with $m = 2 + \gamma^{-2}$ is indicated in the lower part of the figure. Its flux of action ΔW_2 estimated from Eq. (3.35) is orders of magnitude smaller than \hbar , whereas ΔW_3 is found of order \hbar , but $m = 3$ is no longer in a region where (3.35) is reliable. The estimated quantum chaos border resulting from the Cantorus at $m = 2 + \gamma^{-2}$ is given as B_Q . In our numerical data the localization by Cantori is the most consistent scenario to describe the *onset* of dissociation.

For initial energies above B_Q the quantum dissociation probability is also below the classical result, which can be understood as a consequence of incomplete dynamical localization, as explained in Sec. IV B. Dissociation is

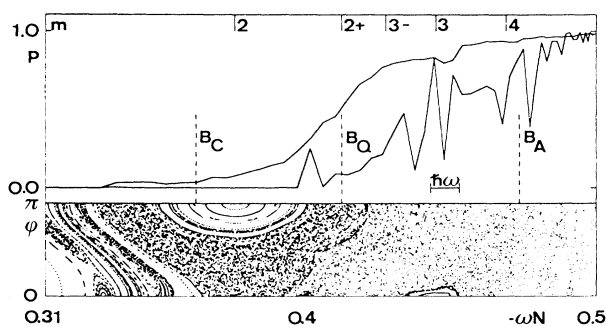


FIG. 10. Dissociation probability after 100 vibration periods (upper curve classical, lower curve quantum) vs initial molecular energy and corresponding phase-space structure. m is the position of the primary resonances and Cantori $2^+ = 2 + \gamma^{-2}$, $3^- = 3 - \gamma^{-2}$, B_C is the classical chaos border, B_Q is the position of the last impenetrable Cantorus, B_A is the Anderson delocalization border. The position of the Cantorus with $m = 2 + \gamma^{-2}$ is included in the lower part of the figure as a dashed line. (The quantum probability is defined for a discrete set of initial energies, the continuous curve merely serves as a guide to the eye.)

merely reduced and not suppressed completely, despite the localization of the Floquet states, because the states $|\lambda\rangle$ have a finite lifetime due to their small but finite overlap with the unbound energy range. Because this overlap increases systematically as the initial energy is moved towards the dissociation energy $\frac{1}{2}$ the dissociation probability increases systematically, on the average. Superimposed on this systematic increase are strong fluctuations which correspond to the fluctuations in the width function shown in Fig. 8. A resonant enhancement of the dissociation probability is seen to occur near the primary resonances $m = 3$ and 4, while the analogous resonance at $m = 2$ is not seen; the latter connects the initial vibrational quantum number $\nu = 48$ with $\nu = 50$ and both states are located below the quantum chaos border. Still, a dissociation peak below B_Q but above the $m = 2$ resonance and the actual Cantorus at $m + \gamma^{-2}$ occurs for an initial energy corresponding to a vibrational quantum number $\nu = 55$. This peak corresponds to the maximum of the width function in Fig. 8 and probably owes its presence to the neighborhood of the classical $m = 2$ resonance. The localization length l_A is also indicated in Fig. 9. Roughly it defines a distance to the dissociation energy $-\omega N = \frac{1}{2}$ within which there is little difference between the classical and the quantum dissociation probability.

D. Scars

As another remarkable feature of Fig. 10 we point out the very low dissociation probabilities surrounding the $m = 3$ and 4 resonances. Likewise pronounced minima of the width function near the $m = 3$ and 4 resonances can be seen in Fig. 8. It is tempting to explain this apparent resonant enhancement of localization by the scarring phenomenon:²³ the enhancement of wave-functions $\langle l|\lambda\rangle$ near the primary unstable periodic orbits of the classical system with winding number m . Such unstable periodic orbits appear together with each stable periodic orbit defining a primary resonance, at the same energy (3.30) but phase shifted by π . Taking into account the recent observation^{24,25} that such scars are extended in phase space along the stable and unstable manifolds of the periodic orbits which surround the classical resonances, one is led to predict that stabilization due to scars should occur immediately above and below the one-photon- m -phonon resonances, in agreement with the resonance structure of Figs. 8 and 10 near $m = 3$ and 4. The resonances at $m = 1, 2$ are not in the chaotic domain, hence the above considerations do not apply, the resonances for $m \geq 5$ are too closely spaced and too close to the dissociation energy to be relevant in the present context. In order to check the scar hypothesis we have determined the Husimi function $|\langle \alpha|\lambda\rangle|^2$, where $|\alpha\rangle$ is a coherent state with $(\Delta N)^2 \simeq (\Delta \varphi)^2 = \hbar/2$. The eigenstates $|\lambda\rangle$ were those having the maximum overlap with the initial states with the selected vibrational quantum numbers $\nu = 64, 65, 66, 67$. These ν values just correspond to the four states near the $m = 3$ resonance in Fig. 10 where the dissociation probability is, respectively, minimal, intermediate, maximal, and again minimal. The result is shown in Fig. 11, where contour lines of the Husimi func-

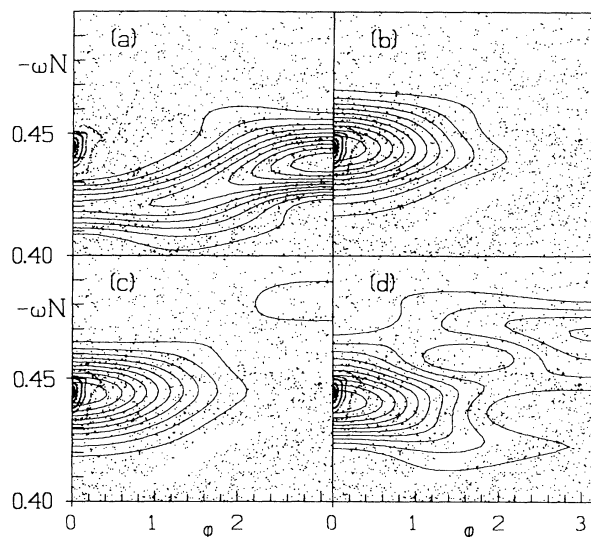


FIG. 11. Husimi distribution (contour lines) and the corresponding phase-space structure for eigenstate $|\lambda\rangle$ of largest overlap with the initial molecular state (a) $\nu=64$, (b) $\nu=65$, (c) $\nu=66$, and (d) $\nu=67$.

tion are plotted on top of the classical phase space structure. It can be seen that the pronounced minimum at $\nu=64$ [Fig. 11(a)] nicely corresponds to a scar, i.e., a wave function with a maximum at the classical resonance energy for $m=3$, but phase shifted by π compared to the stable periodic orbit; i.e., the maximum occurs precisely where the corresponding unstable periodic orbit must be located. The extension of the wave function along the unstable and, to a much lesser extent, stable manifold can also be seen, in agreement with the fact that the energy of this state is below the $m=3$ resonance. Similar results for hydrogen atoms in strong microwave field have been reported in Ref. 26. The eigenstates $|\lambda\rangle$ with maximum overlap to the much less stable initial states with $\nu=65, 66$ [Figs. 11(b) and 11(c)] are centered on the *stable* periodic orbit. Yet, surprisingly, these eigenstates have a larger decay rate than the maximum overlap state of $\nu=64$, which is centered on the corresponding unstable periodic orbit, and also of $\nu=67$. The maximum-overlap state $|\lambda\rangle$ for $\nu=67$ [Fig. 11(d)] is partially centered at the stable periodic orbit for $m=3$, but it has a second maximum at a position of the unstable periodic orbit for $m=4$, i.e., some nontrivial scarring is also present for this state $|\lambda\rangle$, even though, unexpectedly, the scarring is associated with $m=4$. Other states $|\lambda\rangle$ having somewhat smaller but still non-negligible overlap with the same initial state at $\nu=67$ show also scarlike structures, but this time connected with the unstable periodic orbit at $m=3$. All this is consistent with the resonantly enhanced stability of the $\nu=67$ initial state.

It follows from this discussion that the phenomenon of “scarring” may help to interpret some features of the numerical data; however, one should not overlook the fact, that, at least in the present case of relatively large

effective \hbar , this is only possible *a posteriori*, i.e., we could not have predicted the enhanced stability of the initial states with $\nu=65, 66$. It therefore appears that the scar picture in the present case is merely descriptive. In order to test its predictive value it would be necessary to consider cases with much smaller values of the effective \hbar in order to enhance the sensitivity of the eigenstates $|\lambda\rangle$ to classical phase-space structures.

VI. CONCLUSION

We have presented a theoretical approach to multiple-phonon excitation and dissociation of diatomic molecules combining the advantages of the dynamical description by a simple map, which is explicitly known (the Morse map in its simple or its refined form), and the quasis resonant approximation where only levels nearly in resonance with the photonic energy ladder $\hbar\omega l$ above the initial state are taken into account. The quantized map has the attractive feature that it takes into account excitation into the continuum of dissociated states with subsequent deexcitation within the same molecular period. The use of the map has been demonstrated here both in its classical and quantized form. Numerically it provides a very efficient scheme for computation, exceeding in speed alternative schemes based on more direct numerical solutions of the Schrödinger equation. A difficulty connected with the map is the appearance of a molecular time parameter which is related to the physical time in a complicated way. Classically, it is possible to keep trace of this relation for each orbit while iterating the map and to convert all results back to physical time. Quantum mechanically, however, this is as yet not possible in a completely satisfactory way. The best one can do at present is to associate with the internal molecular time parameter an averaged physical time parameter which depends on the instantaneous wave function. This procedure, which we used in Sec. V A, can be expected to work well for states which remain well localized, the case of primary interest in the present work, but it must certainly fail for states spread out in phase space with respect to the action variable. The same problem arises in the largely analogous theoretical approach to Rydberg atoms in strong microwave fields provided by the “Kepler” map.^{3,15,34,37} Clearly a theory avoiding this problem while maintaining the description in terms of the map would be very valuable, but, unfortunately, does not exist so far.

The results obtained in Secs. IV and V show that quantum effects on the classically chaotic dynamics of the driven molecular vibration can be described as localizing effects based on different quasiclassical mechanisms: dynamical localization, localization by Cantori, and localization by scars. We have presented evidence for the presence of all three kinds of localization mechanisms, but it turns out that in each case a realistic physical system, like the one we consider here, presents us with certain difficulties preventing us from reaching an entirely clearcut picture. In the case of dynamical localization one difficulty arises from the finite dimensionality of the subspace formed by the bound states. Dynamical locali-

zation cannot be complete unless the dimension approaches infinity and manifests itself, in the finite-dimensional case, merely as a reduction of the dissociation probability instead of prohibiting dissociation completely. In fact, the ‘‘dissociation border’’ one would predict from the localization length assuming complete localization is much higher than the observed dissociation border, and really describes a regime where the quantum reduction of the dissociation probability essentially disappears. Another difficulty is the appearance of pronounced resonances where one photon can excite an integer number of vibrational quanta. These resonances can lead to sharp increases and decreases of the dissociation probability as a function of initial state or external frequency and are not contained in the simple quasiclassical picture describing dynamical localization in terms of the classical diffusion constant. In further numerical studies³⁸ we found that these resonances are sharper and more pronounced for weaker coupling, i.e., smaller amplitude of the driving field, and become broad and less pronounced as the driving field is increased.

Localization by Cantori best describes the border of dissociation observed in our numerical data such as Fig. 10. This is consistent with earlier results demonstrating Cantorus localization in a similar model.²⁸ However, even this mechanism presents us with practical difficulties. For one, the scaling formula (3.35) for the flux ΔW_m has only limited validity in the scaling region very close to the breakup of the Cantorus. In addition, for the present system the values for ΔW_m turn out to be very strongly dependent on m and it would seem necessary, therefore, to determine the breakup of the last KAM torus not by the primary resonances, which are spaced too far apart, but from higher-order resonances sufficiently close on either side of the KAM torus. While this problem may be overcome a serious shortcoming is the absence, so far, of a theoretical underpinning of the plausible quasi-classical heuristic condition $\Delta W_m > \hbar$ for a Cantorus to become quantum-mechanically penetrable. Further theoretical work deriving this or a similar condition from a quantum theory seems necessary.

Localization by scars is similar to localization by Cantori in that a classical phase-space structure is at its origin. Both are quasiclassical in nature and require the condition $\hbar \ll 1$ for the effective \hbar , i.e., the number of bound states must be very large. However, while Cantorus localization must appear for any initial state with support on one side of the Cantorus only, in order to see a scar it is necessary that the initial state be composed predominantly of wave functions all scarred in a similar way, i.e., by the same unstable periodic orbit. Such initial states are difficult to prepare (either numerically in our model or experimentally). One way to achieve this is to use an adiabatic switch-on of the external field, which makes it possible in principle, to prepare a single Floquet state. In fact, in further numerical experiments with a continuous switch-on of the external field for the parameter values of Fig. 10 we found a significant enhancement of the stabilization in the neighborhood of the $m = 3$ resonance which we have attributed to scars.

We believe that the driven molecule considered here as

an example is rather typical in that various quasiclassical effects occur at the same time and compete with each other. The quasiclassical behavior of such a classically chaotic system is therefore seen to be very rich. The dynamical description in terms of a single quantum map valid in the quasiclassical region and still containing all of these effects together in an easily computable way therefore seems to be particularly useful.

ACKNOWLEDGMENTS

Support of this work by the Deutsche Forschungsgemeinschaft through the Sonderforschungsbereich 237 ‘‘Unordnung und grosse Fluktuationen’’ is gratefully acknowledged.

APPENDIX A: FOURIER TRANSFORM OF THE CLASSICAL UNBOUND MOTION

Here we wish to evaluate the Fourier transforms $V_\mu(I)$ and $W_\mu(I)$ of $x(I, \psi)$ and $p(I, \psi)$, respectively, defined by Eq. (2.16). First we note that Eq. (2.16) implies

$$p(I, \psi) = \sqrt{2H_0(I) - 1} \frac{\partial x(I, \psi)}{\partial \psi}, \quad (\text{A1})$$

which induces the relation

$$W_\mu(I) = -\mu V_\mu(I) \sqrt{2H_0(I) - 1} \quad (\text{A2})$$

between $W_\mu(I)$, defined by Eq. (2.20), and $V_\mu(I)$ defined by

$$x(I, \psi) = 2 \int_0^\infty d\mu V_\mu(I) \cos \mu \psi + |\psi|. \quad (\text{A3})$$

It is therefore sufficient to evaluate the Fourier integral for $V_\mu(I)$

$$V_\mu(I) = \int_{-\infty}^\infty (d\psi/2\pi) [x(I, \psi) - |\psi|] e^{-i\mu\psi}. \quad (\text{A4})$$

Inserting x from Eq. (2.16) and substituting $z = \exp(i\psi)$ we obtain, after some rearrangement of the integrand,

$$\begin{aligned} V_\mu(I) = & -\delta(\mu) \ln \left[\left(\frac{2}{H_0(I)} \right)^{1/2} [2H_0(I) - 1] \right] \\ & + \frac{1}{2\pi} \int_0^\infty dz z^{-i\mu-1} \ln(1 - 2az + z^2) \\ & - \frac{1}{\pi} \int_1^\infty dz z^{-i\mu-1} \ln z \end{aligned} \quad (\text{A5})$$

with $a = 1/\sqrt{2H_0(I)}$. In order to ensure convergence at $z \rightarrow \infty$ we replace μ by $\mu - i\epsilon$. Then the integrals may be done and we obtain, letting $\epsilon \rightarrow +0$,

$$\begin{aligned} V_\mu(I) = & -\delta(\mu) \ln \left[\left(\frac{2}{H_0(I)} \right)^{1/2} [2H_0(I) - 1] \right] + \frac{1}{\pi\mu^2} \\ & - \frac{1}{\pi\mu^2} \cosh \left[\frac{\mu \arccos[-1/\sqrt{2H_0(I)}]}{\sinh(\mu\pi)} \right]. \end{aligned} \quad (\text{A6})$$

The expression (2.20) for $W_\mu(I)$ now follows from Eq. (A2).

**APPENDIX B: SHORT DERIVATION
OF THE HAMILTONIAN
OF THE REFINED MAP AND EXTENSION
TO THE UNBOUND ENERGY RANGE**

We start from the Hamiltonian \tilde{H} , Eq. (3.11). For the purposes of a map from \tilde{t}_n to \tilde{t}_{n+1} the interaction with the external field may be approximated by a symmetry preserving kick at the molecular time $\tilde{t} = \tilde{t}_n = 2\pi n$, when the nuclear distance minimum is passed. Hence we seek the Hamiltonian of the map \tilde{H}_{eff} in the symmetry preserving form

$$\tilde{H}_{\text{eff}} = \tilde{H}_0(N) + \frac{1}{2} \sum_{n=-\infty}^{+\infty} \delta(\tilde{t} - \tilde{t}_n) \left[g(N(\tilde{t} + \epsilon), \varphi(\tilde{t})) + g(N(\tilde{t} - \epsilon), \varphi(\tilde{t})) \right]. \quad (\text{B1})$$

Comparing with the interaction term of Eq. (3.11) we obtain

$$g(N, \varphi) = \frac{g}{\omega} \int_{-\pi}^{\pi} dx h_1(N, x) \sin \left[\frac{\omega x}{\sqrt{1+2\omega N}} + \varphi \right]. \quad (\text{B2})$$

Here we used the fact that in this first-order expression in $g/\sqrt{1+2\omega N}$ we may use the zero-order results for $N(\tilde{t})$ and $\varphi(\tilde{t})$. Substituting the expression for $h_1(N, \tilde{t})$, Eq.

$$h_1(N, x) = -2 \int_0^{\infty} d\mu \left[\frac{\cosh\{\mu \arccos[-1/\sqrt{2H_0(I)}]\}}{\sinh \pi \mu} \right] \sin \mu x \quad (\text{B6})$$

in Eq. (B2), with $I = 1 + \sqrt{|1+2\omega N|}$. Substituting $z = \bar{\lambda}(N)x$, $v = \mu/\bar{\lambda}(N)$ with $\bar{\lambda}(N) = \omega/\sqrt{|1+2\omega N|}$ we arrive at the expression $g(N, \varphi) = \cos \varphi f(N)$ with

$$f(N) = \frac{-4g}{\omega} \int_0^{\pi \bar{\lambda}(N)} dz \int_0^{\infty} dv \sin z \sin v z \left[\frac{\cosh[v \bar{\lambda}(N) \arccos(-1/\sqrt{H_0})]}{\sinh v \bar{\lambda}(N) \pi} \right]. \quad (\text{B7})$$

We are interested in the case $\lambda(N) \gg 1$, where the integral (B7) simplifies and approaches the asymptotic form

$$f(N) \simeq -\frac{4g}{\omega} \int_0^{\infty} dz \int_0^{\infty} dv \sin z \sin v z \times e^{-v \bar{\lambda}(N) \arctan \sqrt{2H_0 - I}}, \quad (\text{B8})$$

which yields

$$f(N) \simeq -\frac{2\pi g}{\omega} \exp \left[\frac{-\omega \arctan \sqrt{|1+2\omega N|}}{\sqrt{|1+2\omega N|}} \right]. \quad (\text{B9})$$

This result can also be obtained directly⁹ from Eq. (B5) by the analytic continuation $\sqrt{1+2\omega N} \rightarrow i\sqrt{-1-2\omega N}$ where it is irrelevant which branch of the square root is taken. The physical reason for this analyticity lies in the fact that bound orbits and unbound orbits are physically indistinguishable in the interaction region around the turning point at the nuclear distance minimum.

(3.7), and using the Fourier expansion (2.14) we arrive at

$$g(N, \varphi) = \frac{-2g}{\omega} \cos \varphi \sum_{m=1}^{\infty} \int_{-\pi}^{\pi} dx \lambda(N)^m \times \sin(mx) \sin \left[\frac{\omega x}{\sqrt{1+2\omega N}} \right], \quad (\text{B3})$$

with

$$\lambda^2(N) = \frac{1 - \sqrt{1+2\omega N}}{1 + \sqrt{1+2\omega N}}. \quad (\text{B4})$$

To evaluate the sum over m approximately we replace it by an integral. This has the consequence that the integrand decays as a function of x over distances $|x| \geq |\ln \lambda(N)|$. Thus for $|\ln \lambda(N)| \ll \pi$ we may extend the x integration to $-\infty \leq x \leq +\infty$ and obtain

$$g(N, \varphi) \simeq \frac{-2\pi g}{\omega} \cos \varphi \lambda(N)^{\omega/\sqrt{1+2\omega N}}. \quad (\text{B5})$$

The effective Hamiltonian now equals Eq. (3.23) with $f(N)$ and $k(N)$ given by Eq. (3.25). While so far the calculations have been restricted to bound states, it is possible within the present approach to extend the effective Hamiltonian also to the unbound domain. We just have to use the Fourier expansion (2.19) and (2.20)

APPENDIX C: KICK OPERATOR

The kick operator may be obtained from

$$K(\lambda) = e^{\lambda[f(N)\cos\varphi + \cos\varphi f(N)]} \quad (\text{C1})$$

for $\lambda = -i(g/2\hbar)$. It is determined by solving the differential equation for the matrix elements $K_{ll'}(\lambda) = \langle l | K(\lambda) | l' \rangle$,

$$\frac{\partial K_{ll'}(\lambda)}{\partial \lambda} = A_{lr} K_{rl'} \quad (\text{C2})$$

with

$$A_{lr} = \frac{1}{2} \sum_r [f(N_l) + f(N_r)] (\delta_{rl-1} + \delta_{rl}). \quad (\text{C3})$$

We note that intermediate states $|r\rangle$ in the unbound energy range contribute to this equation, i.e., the extension of the quantum map to this domain given in Appendix B

is needed here. The matrix A is real, symmetric, tridiagonal, and its diagonal-elements vanish. Its eigenvalues ϵ_n and the orthogonal matrix of its eigenvectors $T_{r,n}$ are constructed numerically. The kick operator then is

$$K_{ll'} = T_{lm} e^{-i(g\epsilon_m/2\hbar)} T_{l'm} . \quad (\text{C4})$$

Even for time-varying g (adiabatic switch on and switch off), the diagonalization has only to be performed once.

- ¹D. W. Lupo and Martin Quack, *Chem. Rev.* **87**, 181 (1987).
²R. V. Ambartsumyan, Yu. A. Groohkov, V. S. Letokhov, and G. N. M. Makarov, *Zh. Eksp. Teor. Fiz.* **69**, 1956 (1975) [*Sov. Phys.—JETP* **42**, 993 (1975)].
³G. Casati, I. Guarneri, and D. L. Shepelyansky, *IEEE J. Quant. Electron.* **24**, 1420 (1988).
⁴R. B. Walker and R. K. Preston, *J. Chem. Phys.* **67**, 2017 (1977).
⁵M. E. Goggin and P. W. Milonni, *Phys. Rev. A* **37**, 796 (1988).
⁶C. Leforestier and R. E. Wyatt, *J. Chem. Phys.* **78**, 2334 (1983).
⁷J. J. Tanner and M. Matti Maricq, *Phys. Rev. A* **40**, 4054 (1989).
⁸T. M. Flosnik and R. E. Wyatt, *Phys. Rev. A* **40**, 5716 (1989).
⁹R. Graham and M. Höhnerbach, *Phys. Rev. Lett.* **64**, 637 (1990); *Proceedings of the Tenth International Vavilov Conference* (Nova Science, New York, 1990).
¹⁰P. M. Morse, *Phys. Rev.* **34**, 57 (1929).
¹¹K. P. Huber and G. Herzberg, *Molecular Spectra and Molecular Structure IV. Constants of Diatomic Molecules* (Van Nostrand Reinhold, New York, 1979).
¹²C. C. Rankin and W. H. Miller, *J. Chem. Phys.* **55**, 3150 (1971).
¹³R. Graham and M. Höhnerbach, in *Fundamentals in Quantum Optics II*, Vol. 192 of *Lecture Notes in Physics*, edited by F. Ehlotzky (Springer, New York, 1987), Sec. 271.
¹⁴R. Graham, *Europhys. Lett.* **7**, 671 (1988).
¹⁵G. Casati, B. V. Chirikov, D. L. Shepelyansky, and I. Guarneri, *Phys. Rep.* **154**, 77 (1987).
¹⁶P. A. Dando and D. Richards (unpublished).
¹⁷B. V. Chirikov, *Phys. Rep.* **52**, 263 (1979).
¹⁸A. J. Lichtenberg and M. A. Lieberman, *Regular and Stochastic Motion*, Vol. 38 of *Applied Mathematical Sciences* (Springer-Verlag, Berlin, 1983).
¹⁹J. M. Greene, *J. Math. Phys.* **20**, 1183 (1979).
²⁰R. S. MacKay and J. D. Meiss, *Phys. Rev. A* **37**, 4702 (1988).
²¹B. V. Chirikov and D. L. Shepelyansky, *Radiofizika* **29**, 1041 (1986).
²²A. Rechester and R. White, *Phys. Rev. Lett.* **44**, 1586 (1980).
²³E. J. Heller, *Phys. Rev. Lett.* **53**, 1515 (1984).
²⁴E. B. Bogomolny, *Physica D* **31**, 169 (1988).
²⁵M. V. Berry, *Proc. R. Soc. London Ser. A* **423**, 219 (1989).
²⁶R. V. Jensen, M. M. Sanders, M. Saraceno, and B. Sundaram, *Phys. Rev. Lett.* **63**, 2771 (1989).
²⁷T. Geisel, G. Radons, and J. Rubner, *Phys. Rev. Lett.* **57**, 2833 (1986).
²⁸R. C. Brown and R. E. Wyatt, *Phys. Rev. Lett.* **57**, 1 (1986).
²⁹J. D. Meiss, *Phys. Rev. Lett.* **62**, 1576 (1989).
³⁰G. Casati, B. V. Chirikov, F. M. Izraelev, and J. Ford, *Lect. Notes Phys.* **93**, 334 (1979).
³¹D. R. Grempel, R. E. Prange, and S. Fishman, *Phys. Rev. Lett.* **49**, 509 (1982).
³²G. Casati, B. V. Chirikov, D. L. Shepelyansky, and I. Guarneri, *Phys. Rev. Lett.* **57**, 823 (1986).
³³D. L. Shepelyansky, *Phys. Rev. Lett.* **56**, 677 (1986), *Physica D* **28**, 103 (1987).
³⁴G. Casati, I. Guarneri, and D. L. Shepelyansky, *Phys. Rev. A* **36**, 3501 (1987).
³⁵R. Graham and M. Höhnerbach (unpublished).
³⁶R. Blümel and U. Smilansky, *Z. Phys. D* **6**, 83 (1987).
³⁷J. G. Leopold and D. Richards (unpublished).
³⁸M. Höhnerbach, Ph.D. thesis, Universität Essen, Hochschulbibliothek, 1990.